Chalcogenide Letters Vol. 20, No. 8, August 2023, p. 563 - 571

Photoluminescence properties of $Ba_{0.7}Sr_{0.3}TiO_3:Sm^{3+}$ modified $K_{0.5}Na_{0.5}NbO_3$ perovskite oxide ceramics

K. W. Sun [a], Z. Liu [b,*], R. X. Wang [b], X. C. Ling [a], J. W. Sun [a]

[a]*College of International Education, Jinling Institute of Technology, Nanjing 211168, China*

[b]*School of Science, Jinling Institute of Technology, Nanjing 211168, China*

$Ba_{0.7}Sr_{0.3}TiO_3:Sm^{3+}$ modified $K_xNa_{(1-x)}NbO_3$ ceramics with perovskite-type structure were synthesized via solid state sintering method. Sm^{3+} ions doping was designed for substituting both A and B sites in the ABO_3 structure, Sm^{3+} doped $Ba_{0.7}Sr_{0.3}TiO_3$ ($Ba_{0.7}Sr_{0.3}TiO_3:Sm^{3+}$) oxide precursor powders with the chemical formula of $Ba_{0.7}Sr_{0.3-x}Sm_x(Ti_{1-x}Sm_x)O_3$ (x=0.005， 0.015， 0.025) were synthesized. Combined $Ba_{0.7}Sr_{0.3}TiO_3:Sm^{3+}$ with $K_{0.5}Na_{0.5}NbO_3$, the perovskite-type solid solution composite ceramics were fabricated via solid phase sintering method. X-Ray diffraction was used for investigating the phase structure of the precursor powders and luminescent composite ceramics. The photoluminescence properties of the Sm^{3+} ions in the $Ba_{0.7}Sr_{0.3}TiO_3$-$K_{0.5}Na_{0.5}NbO_3$ composite ceramic materials were systematically investigated by exploring the effects of composition of the composites, excitation wavelength and temperature on photoluminescence.

(Received May 16, 2023; Accepted August 4, 2023)

Keywords: Perovskite, Sm^{3+}doped, $Ba_{0.7}Sr_{0.3}TiO_3$, $K_{0.5}Na_{0.5}NbO_3$, Photoluminescence

1. Introduction

Inorganic lanthanide rare earth doped luminescent materials have been widely used in lighting, all-solid-state laser, bio-imaging, sensor and catalysis [1-5]. Among these lanthanide rare earth ions, the trivalent lanthanide rare earth ions have abundant energy levels, which make it be possible to generate emissions ranging from ultraviolet to near infrared under excitation of matched wavelength. The typical process of photoluminescence for rare earth ions include upconversion and downshifting process. The upconversion photoluminescence is corresponding to the process of absorbing low energy photons and emitting high energy photons. The common rare earth ions for upconversion photoluminescence are Pr^{3+}, Ho^{3+}, Er^{3+} and Tm^{3+} ions [6-9]. On the contrary, in the process of downshifting photoluminescence, the activated ions absorb high energy photons and emit low energy photons. Plenty of inorganic materials doped with Sm^{3+}, Eu^{3+}, Tb^{3+} and Dy^{3+} have been developed for downshifting photoluminescence [10-13].

* Corresponding author: liuzhen@jit.edu.cn

https://doi.org/10.15251/CL.2023.208.563

In recent years, researchers regulated luminescence properties of rare earth ions via various strategies, including transition metal doping, sensitized rare earth ion doping, applying external electric field, exerting pressure and metal plasmonic effects [14-19]. An important goal for regulating luminescence from rare earths is to achieve high color purity or white light emission in phosphors excited by near ultraviolet or blue light. The current commercial white light light-emitting diodes (LEDs) are generally constructed by combining yellow YAG:Ce^{3+} phosphor with blue LEDs. However, the deficiency of red emission in the photoluminescence emission spectrum of YAG:Ce^{3+} phosphors results in the luminescence of white light LEDs constructed with YAG:Ce^{3+} phosphors and blue light diode is mostly cold white light with color temperature over 5000 K, which is not suited for indoor scenes such as living rooms and classrooms. Therefore, in order to regulate color temperature for warm white light emitting, it is necessary to develop phosphors with red light component. The spectra of Sm^{3+} ions include orange-red light, and its excitation spectra match well with the emission spectra from commercial near ultraviolet (NUV) semiconductor LEDs, which has great prospects in the development of NUV excited white light LEDs [20].

The choice of matrix materials is also very important for rare earth based inorganic phosphors. $Ba_{0.7}Sr_{0.3}TiO_3$ and $K_{0.5}Na_{0.5}NbO_3$ belong to perovskite type oxide solid solution dielectric material. Their excellent ferroelectric properties make them behave well in electronic devices. It is noteworthy that rare earth ions doping can further enhance electrical properties of perovskite ferroelectric oxide materials and integrate photoluminescence properties into electrical materials, which is beneficial for multi-functionalization in single-phase materials. In this work, a series of Sm^{3+} doped ferroelectric perovskite composite ceramics with $Ba_{0.7}Sr_{0.3}TiO_3$ and $K_{0.5}Na_{0.5}NbO_3$ components were developed, and their near ultraviolet light excited photoluminescence properties were systematically studied in the visible region.

2. Experimental procedures

The raw materials include $BaCO_3$ (Aladdin reagent), $SrCO_3$ (Aladdin reagent), TiO_2 (Aladdin reagent), Sm_2O_3 (Aladdin reagent), K_2CO_3 (Aladdin reagent), Na_2CO_3 (Aladdin reagent), Nb_2O_5 (Aladdin reagent) high purity powders. Firstly, the raw materials were weighted according to stoichiometric ratio. Then, the powders were mixed with a small amount of alcohol and ground in an agate mortar for 2 hours. Subsequently, the uniformly mixed raw material slurry were dried and then put into alumina crucible. The target precursor products with the theoretical chemical formula of $Ba_{0.7}Sr_{0.3-x}Sm_{x(}Ti_{1-x}Sm_x)O_3$ (x=0.005, 0.015, 0.025) were synthesized by high temperature solid phase sintering method. In the process of high temperature solid phase reactive synthesis, the powders were heated to 900 °C with a heating rate of 5 °C/min, and hold at 900 °C for 3 hours. After the solid state reaction, the powders were naturally cooled to room temperature for obtaining $Ba_{0.7}Sr_{0.3-x}Sm_{x(}Ti_{1-x}Sm_x)O_3$ precursor sample. The $K_{0.5}Na_{0.5}NbO_3$ precursor powders were prepared via similar process as that of $Ba_{0.7}Sr_{0.3-x}Sm_{x(}Ti_{1-x}Sm_x)O_3$. For obtaining $Ba_{0.7}Sr_{0.3}TiO_3$:Sm^{3+} modified $K_{0.5}Na_{0.5}NbO_3$ composite functional ceramics, the $Ba_{0.7}Sr_{0.275}Sm_{0.025}(Ti_{0.975}Sm_{0.025})O_3$ precursor powders were blended with $K_{0.5}Na_{0.5}NbO_3$ precursor powders according to a mole percentage of (5%, 10%, 20%, 30%) (abbreviated as KNN-yBSTSm, y=0.05, 0.1, 0.2, 0.3). After following the processes of grinding, glueing and molding, the pallets

were sintered at 1150 °C for 2 hours, followed by naturally cooling to room temperature for obtaining the designed perovskite oxide ceramics.

The phase structure of samples were characterized by X-Ray diffraction (Bruker D8 X-ray diffractometer). The photoluminescence properties of the phosphors doped with various content of rare earth ions were investigated by steady-state photoluminescence emission spectra, which was recorded on PerkinsElmer FL6500 fluorescence spectrometer equipped with an 80 W pulsed xenon lamp. The photoluminescence excitation spectra of ceramic samples monitored at 598 nm were recorded in the excitation wavelength range from 250 nm to 500 nm. The photoluminescence emission spectra of samples excited by different excitation wavelengths and that of solid solution ceramic samples with different components under the excitation of 408 nm were collected in the emission wavelength range from 520 nm to 720 nm. Moreover, the temperature dependent photoluminescence properties of composite ceramic were investigated via analysis of the emission spectra of sample at various temperature. The emission intensity as a function of temperature was fitted by theoretical model for thermal quenching.

3. Results and discussion

Fig. 1 depicts the XRD patterns of synthesized $Ba_{0.7}Sr_{0.3-x}Sm_x(Ti_{1-x}Sm_x)O_3$ (x=0.005, 0.015, 0.025) precursor powder in the 2θ range from 10° to 70°. It can be clearly seen that the dominate diffraction peaks can be matched with standard card PDF70-3628, indicating the synthesized powders are mainly solid solution with perovskite phase. The position of diffraction peaks does not shift significantly with increasing Sm^{3+} doping concentrations. It is reasonable to explain this phenomenon by considering the effects of ion radius on lattice structure. Considering Sm^{3+} (1.24Å, CN=12) ions have smaller ion radii than Ba^{2+} ions (1.61Å, CN=12), resulting in shrinkage of lattice and decreacement of lattice constant for host matrix when Sm^{3+} substitute Ba^{2+} ions. However, when Sm^{3+} enter into the sites of Ti^{4+} ions, the lattice constant of host matrix has inverse trend compared with that situation of Ba^{2+} site substituting due to Sm^{3+} (0.958Å, CN=6) ions have larger ion radii than Ti^{4+} ions (0.605Å, CN=6). With the consideration of charge balance in the designed chemical formula, the Sm^{3+} dopant ions equally incorporated into Ba^{2+} and Ti^{4+} sites of $BaTiO_3$ host matrix. The effects of different doping sites on lattice constant have opposite trends and offset each other's contribution, resulting in no singnificant peak shifting shown in the diffraction pattern.

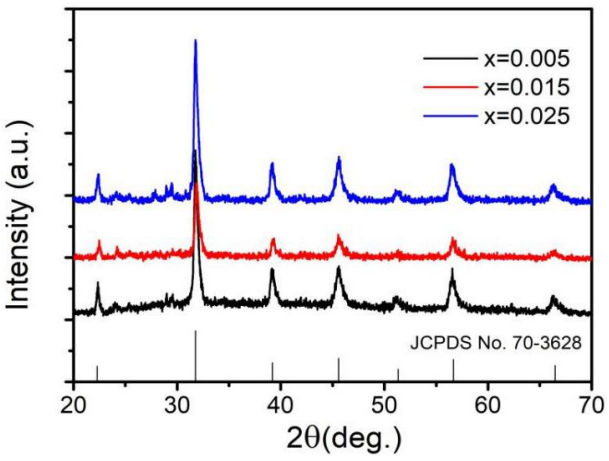

Fig. 1. X-ray diffraction patterns of $Ba_{0.7}Sr_{0.3-x}Sm_x(Ti_{1-x}Sm_x)O_3$ (x=0.005, 0.015, 0.025) precursor powders.

The X-Ray diffraction patterns of (1-y)$K_{0.5}Na_{0.5}NbO_3$- y$Ba_{0.7}Sr_{0.275}Sm_{0.025}(Ti_{0.975}Sm_{0.025})O_3$ (y=0.05, 0.1, 0.2, 0.3) (abbreviated as KNN-yBSTSm) ceramics were shown in Fig. 2. As shown in Fig. 2, the diffraction patterns of synthesized ceramics were matched well with perovskite structure when the proportion of $Ba_{0.7}Sr_{0.275}Sm_{0.025}(Ti_{0.975}Sm_{0.025})O_3$ is lower 20 mol%. However, when the content of $Ba_{0.7}Sr_{0.275}Sm_{0.025}(Ti_{0.975}Sm_{0.025})O_3$ exceeds 30 mol%, some diffraction peaks corresponding to impurity phase appear in 2θ range from 25° to 30°. It suggests that the high concentration of Sm^{3+} ions in the KNN-yBSTSm composite ceramics may result in the formation of a small amount of non-perovskite phase rare earth titanates and niobates.

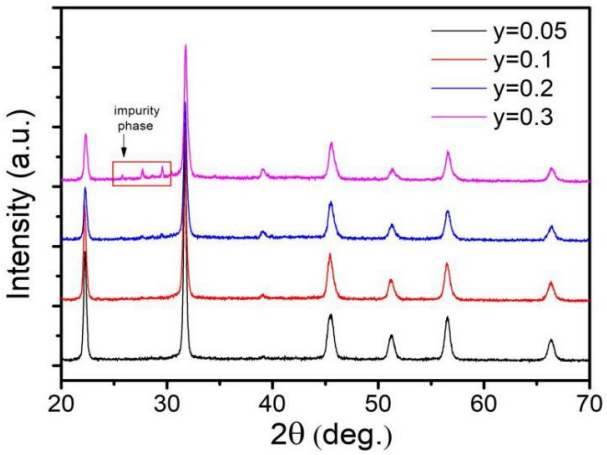

Fig. 2. X-ray diffraction pattern of (1-y)$K_{0.5}Na_{0.5}NbO_3$-y$Ba_{0.7}Sr_{0.275}Sm_{0.025}(Ti_{0.975}Sm_{0.025})O_3$(y=0.05, 0.1, 0.2, 0.3) ceramics.

For investigating the photoluminescence properties of Sm^{3+} ions in $K_{0.5}Na_{0.5}NbO_3$-y$Ba_{0.7}Sr_{0.3}TiO_3$ based solid solution ceramics, the excitation spectrum of $K_{0.5}Na_{0.5}NbO_3$-0.2$Ba_{0.7}Sr_{0.275}Sm_{0.025}(Ti_{0.975}Sm_{0.025})O_3$ ceramic in the spectral range from 240 nm to 500 nm was recorded via monitoring 598 nm emission. As shown in Fig. 3, there are five characteristic excitation bands, centering at 408 nm, 421 nm, 440 nm, 465 nm and 479 nm, respectively. These excitation bands are corresponded to transitions of $^6H_{5/2}\rightarrow{}^4F_{7/2}$, $^4H_{5/2}\rightarrow{}^6P_{5/2}$, $^6H_{5/2}\rightarrow{}^4G_{9/2}$, $^6H_{5/2}\rightarrow{}^4I_{13/2}$, $^6H_{5/2}\rightarrow{}^4I_{11/2}$, which are resulted from abundant electronic configurations of Sm^{3+} ions and matched energy of exciting light with energy gaps between ground state and excited state levels of Sm^{3+}. The strongest exciting wavelength is 408 nm, which indicates the photoluminescence emission can be efficiently excited by near ultraviolet light. In addition, the near ultraviolet light at 408 nm is well matched with the emission spectra of commercial semiconductor chips, illustrating the synthesized phosphors have great potential in applications of near ultraviolet excited phosphor converted LEDs.

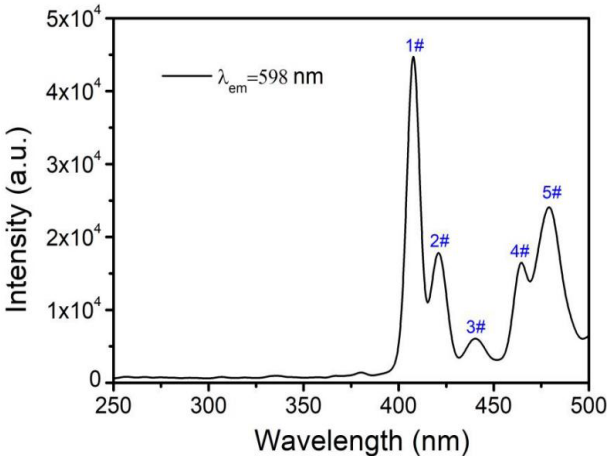

Fig. 3. Photoluminescence excitation spectrum of $K_{0.5}Na_{0.5}NbO_3$-0.2$Ba_{0.7}Sr_{0.275}Sm_{0.025}(Ti_{0.975}Sm_{0.025})O_3$ ceramic monitored at 598 nm.

Fig. 4 displays the photoluminescence emission spectra (ranged from 520 nm to 750 nm) of $K_{0.5}Na_{0.5}NbO_3$-0.2$Ba_{0.7}Sr_{0.275}Sm_{0.025}(Ti_{0.975}Sm_{0.025})O_3$ ceramic under excitation of five different excitation wavelengths. As shown, the emission bands are located around 563 nm, 598 nm, 644 nm and 703 nm, respectively. These emission bands can be ascribed to intrinsic f-f transitions of Sm^{3+} ions. According to energy levels of Sm^{3+} ions, these transitions are corresponded to magnetic dipole transition ($^4G_{5/2}\rightarrow{}^6H_{5/2}$), partial magnetic dipole transition ($^4G_{5/2}\rightarrow{}^6H_{7/2}$) and electric dipole transitions ($^4G_{5/2}\rightarrow{}^6H_{9/2}$, $^6H_{9/2}$), respectively. The emission intensity reaches the maximum when the ceramic was excited by 408 nm, which coincides with the optimum excited wavelength as suggested by the excitation spectrum. These results confirmed that the near ultraviolet light near 408 nm is most efficient excitation light for 598 nm emission from Sm^{3+} ions in $K_{0.5}Na_{0.5}NbO_3$-0.2$Ba_{0.7}Sr_{0.275}Sm_{0.025}(Ti_{0.975}Sm_{0.025})O_3$ ceramic. There is no significant shift in the positions of emission bands, indicating similar excited state energy levels were populated by absorbing energy from irradiated high energy photons, and similar mechanisms for luminescence of $K_{0.5}Na_{0.5}NbO_3$-0.2$Ba_{0.7}Sr_{0.275}Sm_{0.025}(Ti_{0.975}Sm_{0.025})O_3$ ceramic under excitation of light at several different excited wavelengths.

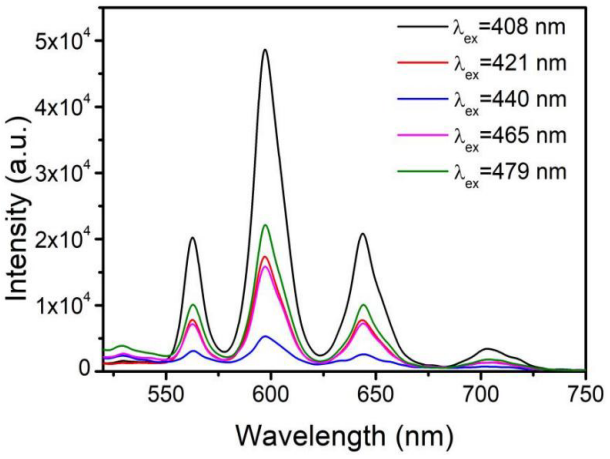

Fig. 4. Photoluminescence emission spectrum of $K_{0.5}Na_{0.5}NbO_3$-0.2$Ba_{0.7}Sr_{0.275}Sm_{0.025}(Ti_{0.975}Sm_{0.025})O_3$ excited at different wavelength.

In order to investigate the effect of components on photoluminescence of synthesized $K_{0.5}Na_{0.5}NbO_3$ based ceramics, under excitation of 408 nm, the emission spectra of $K_{0.5}Na_{0.5}NbO_3$-y$Ba_{0.7}Sr_{0.275}Sm_{0.025}(Ti_{0.975}Sm_{0.025})O_3$ (y = 0.05，0.1，0.2，0.3) ceramics were recorded in the spectral range from 520 nm to 750 nm. As displayed in Fig. 5, the positions of emission bands show no shift with increase of $Ba_{0.7}Sr_{0.275}Sm_{0.025}(Ti_{0.975}Sm_{0.025})O_3$. However, the intensities of emission bands firstly increase with elevation of the proportion of $Ba_{0.7}Sr_{0.275}Sm_{0.025}(Ti_{0.975}Sm_{0.025})O_3$ in composite ceramics and then slightly decrease when y exceeds 0.2. It suggests that the $K_{0.5}Na_{0.5}NbO_3$-0.2$Ba_{0.7}Sr_{0.275}Sm_{0.025}(Ti_{0.975}Sm_{0.025})O_3$ ceramic has the best photoluminescence performance for synthesized composite ceramics. This phenomena is coincided with the results of X-ray diffraction characterization, in which no impurity phase appears until y reaches 0.2.

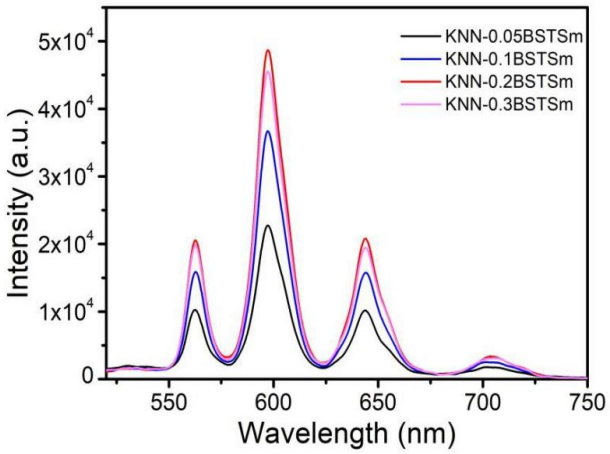

Fig. 5. Photoluminescence emission spectrum of $K_{0.5}Na_{0.5}NbO_3$-y$Ba_{0.7}Sr_{0.275}Sm_{0.025}(Ti_{0.975}Sm_{0.025})O_3$ ceramics (y = 0.05，0.1，0.2，0.3).

The thermal stability for photoluminescence is important for evaluation of high performance phosphors. For investigating the thermal stability of synthesized Sm^{3+} activated composite ceramic, the photoluminescence emission spectra of ceramic with optimum composition are collected in temperature range from 293 K to 453 K. Fig. 6 displays the temperature dependent photoluminescence emission spectra of 408 nm light excited $K_{0.5}Na_{0.5}NbO_3$-0.2$Ba_{0.7}Sr_{0.275}Sm_{0.025}(Ti_{0.975}Sm_{0.025})O_3$ ceramic in spectral range from 520 nm to 750 nm. It can be seen that the emission intensity decrease with elevation of temperature. This is due to the enhancement of electron-phonon interactions as the temperature increase. Thermal activated electrons jump across energy barrier and pass the cross point between excited state energy level and ground state energy level, and subsequently return to the ground state energy level by non-radiative transition, resulting in luminescence quenching.

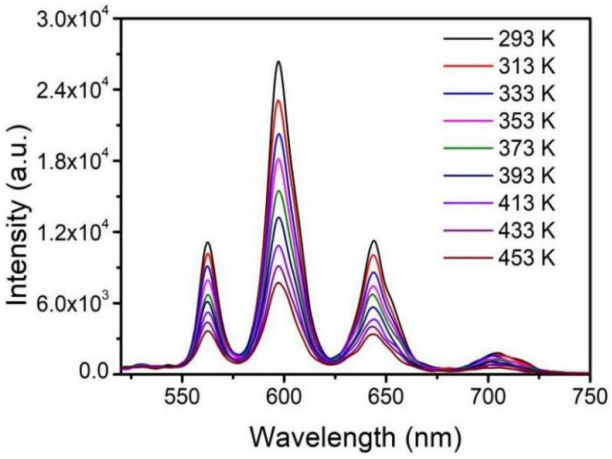

Fig. 6. Temperature dependent photoluminescence emission spectra of 408 nm light excited $K_{0.5}Na_{0.5}NbO_3$-$0.2Ba_{0.7}Sr_{0.275}Sm_{0.025}(Ti_{0.975}Sm_{0.025})O_3$ *ceramic.*

For further understanding the thermal quenching behavior of photoluminescence resulted from activated Sm^{3+} ions, the normalized intensity of emission band at 598 nm as a function of temperature was analysed via theoretical model. As illustrated in Fig. 7, the temperature dependent emission intensity in range from 293 K to 453 K can be well fitted by Arrhennius formula. (Blue square dots represents the experimental data and the red line is the fitting curve).

$$I = \frac{I_0}{1+Cexp(-\frac{\Delta E}{kT})} \quad (1)$$

Here, T is absolute temperature, I is integral emission intensity at T K, I_0 represents integral emission intensity at 0 K, ΔE is activation energy for thermal quenching, C is fitting constant, k is the Boltzmann constant [21].

It can also be seen that the emission intensity at 420 K remains 40 % of that at 293 K. According to the fitting results, the activation energy for thermal quenching of luminescent Sm^{3+} ions is 0.1748 eV, indicating the synthesized Sm^{3+} activated phosphors have good thermal stability for photoluminescence. Combined with the intrinsic ferroelectric properties of $K_{0.5}Na_{0.5}NbO_3$ based ceramics, the $K_{0.5}Na_{0.5}NbO_3$-$0.2Ba_{0.7}Sr_{0.275}Sm_{0.025}(Ti_{0.975}Sm_{0.025})O_3$ may have great potential for applications of lighting and optoelectronic devices.

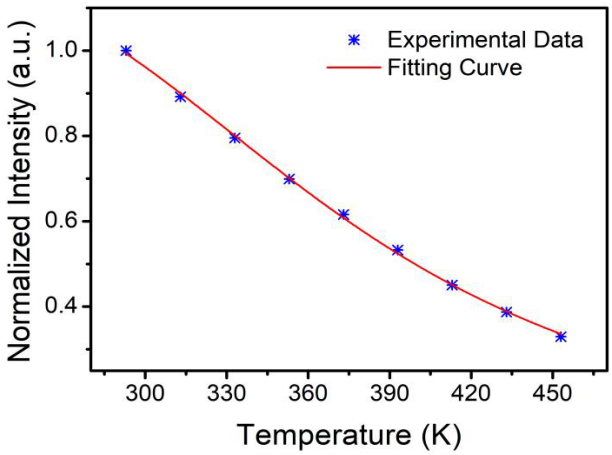

Fig. 7. Temperature dependent integral intensity of 598 nm emission.

4. Conclusion

A series of $Ba_{0.7}Sr_{0.3}TiO_3:Sm^{3+}$ modified $K_{0.5}Na_{0.5}NbO_3$ based oxide ceramics were synthesized via solid phase sintering method. The synthesized ceramics show perovskite phase with no impurity phase until the mole proportion of $Ba_{0.7}Sr_{0.275}Sm_{0.025}(Ti_{0.975}Sm_{0.025})O_3$ reaches 20 %, which is also the optimal component for photoluminescence. The excitation spectra of samples can be matched with the emission of commercial semiconductor near ultraviolet LEDs, suggesting the potential in near ultraviolet excited phosphor converted LEDs. Under excitation of 408 nm, the synthesized Sm^{3+} activated phosphors exhibited good thermal stability with thermal activation energy of 0.1748 eV. Meanwhile, the emission intensity at 420 K remain its 40 % of that at 293 K. All the results suggest the $K_{0.5}Na_{0.5}NbO_3$-$0.2Ba_{0.7}Sr_{0.275}Sm_{0.025}(Ti_{0.975}Sm_{0.025})O_3$ based phosphors have great potential applications in lighting.

Acknowledgements

This work is financially supported by the Research Start-up Program of Jinling Institute of Technology (jit-b-202054), Jiangsu Province's Double Innovation Plan (JSSCBS20210616), National Natural Science Foundation of China (Grant No.11804150), Natural Science Foundation of Jiangsu Province (BK20201111), Entrepreneurship Training Program for College Students of Jiangsu Province (202213573110Y).

References

[1] G. Li, Y. Tian, Y. Zhao et al., Chemical Society Review, 2015, (44): 8688-8713; https://doi.org/10.1039/C4CS00446A

[2] F. Peng, W. P. Liu, Q. L. Zhang, Journal of Luminescence, 2018, (201): 176-181; https://doi.org/10.1016/j.jlumin.2018.04.034

[3] X. Xu, Z. Zhou, Y. Liu et al., APL Photonics, 2019, (4): 026104; https://doi.org/10.1063/1.5053608

[4] A. K. Soni, V. K. Rai, Chemical Physics Letters, 2017, (667): 226-232; https://doi.org/10.1016/j.cplett.2016.12.002

[5] W. Gao, Y. Q. Wu, G. X. Lu, Catalysis Science & Technology, 2020, (10): 2389-2397; https://doi.org/10.1039/D0CY00256A

[6] X. Y. Han, C. Q. Hu, J. M. Wu et al., Systematical Site Investigation and Temperature Sensing in Pr3+-doped M3RE4O9 (M = Sr and Ba; RE = Sc, Y, Lu)

[7] Z. Liu, H. W. Deng, D. H. Chen, Ceramics International, 2019, (45): 13235-13241; https://doi.org/10.1016/j.ceramint.2019.04.009

[8] H. N. Liu, J. T. Wang, H. Wang et al., Ceramics International, 2022, (48): 4230-4237; https://doi.org/10.1016/j.ceramint.2021.10.215

[9] W. Y. Ge, M. M. Xu, J. D. Shi et al., Chemical Engineering Journal, 2020, (391): 123546; https://doi.org/10.1016/j.cej.2019.123546

[10] S. Wang, H. Zhang, T. Wang et al., Journal of Alloys and Compounds 2020, (823): 153822; https://doi.org/10.1016/j.jallcom.2020.153822

[11] Y. Gao, P. F. Jiang, R. H. Cong et al., Journal of Luminescence, 2022, (251): 119161; https://doi.org/10.1016/j.jlumin.2022.119161

[12] W. Piotrowski, M. Kuchowicz, M. Dramicanin et al., Chemical Engineering Journal, 2022, (428): 131165; https://doi.org/10.1016/j.cej.2021.131165

[13] C. Lin, H. Wang, P. Wang et al., Journal of the American Ceramic Society, 2021, (104): 903-916; https://doi.org/10.1111/jace.17533

[14] J. C. Zhou, M. T. Chen, J. X. Zhang et al., Chemical Engineering Journal, 2021, (426): 131869; https://doi.org/10.1016/j.cej.2021.131869

[15] N. Gao, Y. F. Yang, S. K. Shi et al., Journal of Rare Earths, 2020, (38): 1273-1280; https://doi.org/10.1016/j.jre.2019.09.014

[16] A. Shandilya, R. S. Yadav, A. K. Gupta et al., Materials Chemistry and Physics, 2021, (264): 124441; https://doi.org/10.1016/j.matchemphys.2021.124441

[17] J. H. Hao, Y. Zhang, X. H. Wei, Angewandte Chemie International Edition, 2011, (50): 6876; https://doi.org/10.1002/anie.201101374

[18] X. Wang, C. N. Xu, H. Yamada et al., Advanced Materials, 2005, (17): 1254-1258; https://doi.org/10.1002/adma.200401406

[19] J. C. Yin, H. T. Zheng, A. M. Li et al., Nanotechnology, 2021, (32): 435201; https://doi.org/10.1088/1361-6528/ac12ed

[20] W. Y. Zhao, H. X. Wen, X. D. Yang et al., Materials Letters, 2020, (261): 127104; https://doi.org/10.1016/j.matlet.2019.127104

[21] Z. Liu, G. C. Jiang, R. X. Wang et al., Ceramics International, 2016, (42): 11309-11313; https://doi.org/10.1016/j.ceramint.2016.04.049